Research Square

Preprints are preliminary reports that have not undergone peer review.
They should not be considered conclusive, used to inform clinical practice,
or referenced by the media as validated information.

Serglycin as a Preliminary Candidate Biomarker in GNE Myopathy Associated with Impaired Secretion and Autophagy Dysregulation

Alexa Derksen
University of Ottawa
Vera Dobelmann
Düsseldorf University Hospital
Andreas Hentschel
Leibniz-Institut für Analytische Wissenschaften – ISAS – e.V
Stephen Baird
Children's Hospital of Eastern Ontario Research Institute
Stephen Henry Holland
University of Ottawa
Lei Chen
University of Duisburg-Essen
Tobias Ruck
Düsseldorf University Hospital
Rüdiger Horstkorte
Martin Luther University Halle-Wittenberg
Jason D. Doles
Indiana University
Margherita Milone
Mayo Clinic
Sally Spendiff
Children's Hospital of Eastern Ontario Research Institute
Andreas Roos
Children's Hospital of Eastern Ontario Research Institute
Hanns Lochmüller
hlochmuller@toh.ca

Children's Hospital of Eastern Ontario Research Institute

Research Article

Keywords: GNE myopathy, serglycin, biomarker discovery

Posted Date: June 13th, 2026

DOI: https://doi.org/10.21203/rs.3.rs-9791335/v1

License: This work is licensed under a Creative Commons Attribution 4.0 International License.
Read Full License

Additional Declarations: No competing interests reported.

Version of Record: A version of this preprint was published at Acta Neuropathologica Communications on September 9th, 2026. See the published version at https://doi.org/10.1186/s40478-026-02422-8.

Abstract

GNE myopathy (GNEM) is a neuromuscular disorder caused by biallelic mutations in the gene *GNE*, which encodes a bifunctional enzyme essential for the biosynthesis of sialic acid. Despite extensive characterization, no effective therapies or validated biomarkers exist, and the molecular mechanisms driving disease pathology remain poorly understood. This study identifies the proteoglycan serglycin as a preliminary candidate biomarker in GNEM and investigates the mechanisms underlying its dysregulation. Proteomic analysis of serum samples from GNEM patients revealed reduced circulating serglycin levels. In contrast, increased intracellular serglycin was observed in *GNE* knockout and GNEM patient iPSC-derived myoblasts, suggesting impaired secretion and/or degradation. To investigate the basis of this accumulation, intracellular trafficking and autophagic pathways were examined. Proteomic profiling from HEK *GNE* knockout cells revealed alterations in pathways involved in membrane trafficking, Golgi function, and glycoprotein processing, consistent with broader disruptions in the secretory system that may impair serglycin export and contribute to its intracellular retention. In GNEM iPSC-derived myoblasts, serglycin overlapped with LAMP1-positive lysosomal compartments and the ER-phagy receptor FAM134B, suggesting association with lysosomal and ER-phagy related pathways. Functional assays further indicated impaired autophagic flux in mutant cells. Together, these findings support a model in which combined defects in secretion and autophagic clearance contribute to intracellular serglycin accumulation and reduced circulating levels. This study identifies serglycin as a potential circulating biomarker for GNEM and highlights dysregulation of secretory and degradative pathways as converging features of disease pathology.

Introduction

GNE myopathy (GNEM) is a rare, autosomal recessive neuromuscular disorder, caused by mutations in the gene *GNE*. The *GNE* gene encodes the bifunctional enzyme UDP-*N*-acetylglucosamine 2-epimerase/*N*-acetylmannosamine kinase, which catalyzes sequential steps in the biosynthesis of sialic acid [1–3]. Although the genetic basis of GNEM was identified more than 25 years ago [1], the molecular mechanisms driving disease pathogenesis remain incompletely understood.

GNEM has long been hypothesized to result from the hyposialylation of essential muscle glycoconjugates [4–7]. However, clinical trials employing sialic acid supplementation or related approaches have demonstrated limited or no clinical benefit, suggesting that hyposialylation alone may not fully account for disease onset or progression [8–12]. The lack of clear positive results may reflect insufficient sensitivity of current clinical outcome measures, inadequate delivery of therapeutic compounds to affected muscle tissue, or the possibility that hyposialylation represents only one component of a more complex pathogenic process [8, 13]. Compounding these challenges is the absence of validated diagnostic and disease-progression biomarkers, which remains a major barrier to therapeutic development [13]. The need for robust biomarkers is particularly critical in rare disease, where sensitive and minimally invasive markers could enable earlier disease detection, reduce reliance

on costly and labour-intensive diagnostic testing, and provide reliable longitudinal measures to assess disease progression [14–16].

Emerging evidence suggests that GNE dysfunction affects multiple cellular processes beyond sialic acid biosynthesis [17], including cytoskeletal organization [18–23], oxidative stress responses [24, 25], endoplasmic reticulum stress signaling [26–29], myogenesis [30] and autophagy [30–33]. A defining pathological feature of GNEM is the presence of rimmed (autophagic) vacuoles in affected muscle fibers on muscle biopsy [34]. These structures consist of clusters of autophagic vacuoles and myeloid-like bodies and contain intracellular aggregates of proteins such as amyloid-β, α-synuclein, and abnormally phosphorylated tau. Consistent with this pathology, GNEM muscle biopsies frequently show accumulation of macroautophagy markers, including LC3 and p62/SQSTM1, along with increased expression of lysosomal proteins such as LAMP1 and LAMP2 which may localize to rimmed vacuoles [4, 35, 36]. Similar disruptions in autophagy and lysosomal pathways have been reported across multiple cellular models of GNEM, including patient-derived fibroblasts [31], induced pluripotent stem cell (iPSC)-derived myogenic progenitors [30], and other engineered immortalized cell systems [27, 32, 33, 37]. However, the precise mechanisms linking GNE dysfunction to autophagy impairment remain unclear, including whether these defects arise directly from GNE dysfunction, altered sialylation states, or broader disruptions in cellular proteostasis.

Serglycin is a small intracellular proteoglycan best characterized for its role in the storage and regulated secretion of bioactive molecules, particularly in hematopoietic and endothelial cells [38, 39]. Structurally, serglycin consists of a small core protein containing a serine/glycine-rich repeat region that serves as the attachment site for highly sulfated glycosaminoglycan (GAG) chains [38]. Recently, serglycin has been shown to be expressed and secreted by human skeletal muscle where it may participate in extracellular matrix remodeling and stress-responsive signaling [40]. In myoblasts, serglycin localizes to perinuclear cytoplasmic vesicles and traffics through the classical secretory pathway, suggesting that its intracellular distribution may be affected by disruptions in vesicle trafficking and protein quality control processes [40].

In this study, we investigated whether serglycin is dysregulated in GNEM and evaluated its potential as a candidate circulating biomarker. Using patient serum samples and cellular models of GNEM, we characterized serglycin abundance, localization, and its relationship to secretory trafficking and autophagy-lysosomal pathways.

Methods

Sample preparation for LC-MS/MS for patient serum samples

Snap frozen serum samples were gently thawed at 4°C. After short vortex and spin down, 10µl of each serum sample were added to 190µl of lysis buffer (50mM TEAB, pH 7.8, 5% SDS, supplemented with

cOmplete™ ULTRA protease inhibitor cocktail, Roche Cat no. 05892970001). Protein concentration was quantified using the BCA assay according to the manufacturer's instructions.

Reduction of disulfide bonds was performed by incubation with 10mM TCEP at 37°C for 30 minutes, followed by alkylation with 15 mM IAA at room temperature for 30 minutes in the dark. For proteolytic digestion, 100µg of total protein from each sample was processed using the S-Trap protocol (Protifi) with a protein-to-trypsin ratio of 20:1. Digestion was carried out for 2 hours at 47°C, and the reaction was terminated by acidification with formic acid to a final pH below 3.

Sample preparation and protein digestion for HEK WT and GNE knockout proteomics

Frozen HEK WT and *GNE* KO cell pellets were treated with 200µL of lysis buffer (50mM TEAB, pH 7.8, 5% SDS, supplemented with cOmplete™ ULTRA protease inhibitor cocktail, Roche Cat no. 05892970001), followed by mechanical disruption using a Bioruptor® sonication system (Diagenode) for 10 minutes (30 seconds on/30 seconds off, 10 cycles) at 4°C. To achieve complete homogenization, samples were additionally subjected to probe sonication (30 seconds, 1 second on/1 second off, amplitude 40%), and insoluble material was removed by centrifugation (20,000g for 15 minutes at 4°C). Protein concentration in the cleared supernatant was quantified using the BCA assay according to the manufacturer's instructions.

Reduction of disulfide bonds was performed by incubation with 10mM TCEP at 37°C for 30 minutes, followed by alkylation with 15mM IAA at room temperature for 30 minutes in the dark. For proteolytic digestion, 100µg of total protein from each sample was processed using the S-Trap protocol (Protifi) with a protein-to-trypsin ratio of 20:1. Digestion was carried out for 2 hours at 42°C, and the reaction was terminated by acidification with formic acid to a final pH below 3.

Check for proteolysis efficiency

The completeness of proteolytic cleavage was evaluated following desalting by monolithic column separation (PepSwift PS-DVB PL-CAP200-PM, Dionex) using an UltiMate 3000 HPLC system (Dionex, Germering, Germany). For each analysis, 1µg of digest was injected directly. Chromatographic separation was achieved with a binary gradient (solvent A: 0.1% TFA; solvent B: 0.08% TFA in 84% acetonitrile), starting at 5–12% B over 5 minutes, followed by 12–50% B over 15 minutes, at a flow rate of 2.2 µL/min and 60°C. UV detection was carried out at 214 nm [41].

DIA-LC-MS/MS analysis for HEK cell lysates and patient serum samples

All samples were subjected to analysis using an UltiMate 3000 RSLC nano UHPLC system paired with a QExactive HF mass spectrometer, consistently applying 1µg of peptide per sample. Initially, the samples were loaded onto a 75 µm x 2 cm, 100 Å, C18 pre-column at a flow rate of 20 µl/min for 20 minutes.

Subsequently, separation was carried out on a 75 µm x 50 cm, 100 Å, C18 main column with a flow rate of 250 nl/min, utilizing a linear gradient composed of solution A (99.9% water, 0.1% formic acid) and solution B (84% acetonitrile, 15.9% water, 0.1% formic acid). The gradient length was set to 120 minutes (3–45% solution B). The gradient protocol included: 3% solution B for 20 minutes, 3–35% over 120 minutes, followed by three wash steps each reaching 95% solution B for 3 minutes. Post-wash, the instrument was allowed to equilibrate for 20 minutes. MS data acquisition was performed in DIA (data-independent acquisition) mode, utilizing an in-house developed spectral library. Each sample was spiked with an appropriate quantity of iRT standard (Biognosys). Full MS scans were recorded from 300–1100 m/z at a resolution of 60,000 (Orbitrap), using the polysiloxane ion at 445.12002 m/z as a lock mass. The automatic gain control (AGC) was set at 3E6, with a maximum injection time of 20 milliseconds. Full MS scans were succeeded by 23 DIA windows, each covering 28 m/z with a 1 m/z overlap, starting at 400 m/z, acquired at a resolution of 30,000 (Orbitrap) with an AGC of 3E6 and a normalized collision energy (nCE) of 27 (CID).

Analysis of DIA data from HEK cell lysates and patient serum samples

For the analysis of the samples acquired with nano-LC-MS/MS in DIA mode, the data was introduced to the Spectronaut software (Biognosys) and analyzed with a direct DIA-based search. As library the human proteome data was selected from UniProt (www.uniprot.org) containing 20,405 entries (downloaded on January 23rd 2023). Search and extraction settings were kept as standard (BGS Factory settings) Normalization was done by the software, using global normalization based on the median. For reliable label-free quantification, only proteins identified with ≥ 2 unique peptides were considered for further analysis. Subsequently, the average normalized abundances (determined using Spectronaut) were calculated for each protein and used to determine the ratio between the leukocytes from the patients and the corresponding controls. Finally, a Student's t-test with p-values was calculated in MS Excel. Only proteins with a p-value of ≤ 0.05 and an abundance ratio of ≥ 2 or ≤ 0.5 (up-regulated as well as down-regulated) were considered as finally regulated.

ELISA

Serglycin levels were measured in serum samples derived from GNEM patients and controls using the “Human SRGN ELISA kit” (AssayGenie Cat no. HUES03361). The assay was performed according to the manufacturers’ instructions, and the samples were used at a dilution of 1:2000. Serum samples were stored at -80°C and thawed on ice prior to analysis. Samples were measured in technical duplicates, and repeated freeze–thaw cycles were avoided. Standard curves were generated for each plate using recombinant protein standards provided with the respective kit. Absorbance was measured using a microplate reader at the recommended wavelength, and protein concentrations were calculated by interpolation from the corresponding standard curves.

Antibodies

The antibodies used were obtained from the following companies: Serglycin H-9 (Santa Cruz Biotechnology Cat no. sc-393521) (Immunoblot (IB) 1:500), Serglycin C-11 (Santa Cruz Biotechnology Cat no. sc-374657) (Immunofluorescence (IF) 1:100), LAMP1 (New England Biolabs Cat no. 9091S) (IF 1:300), FAM134B (ProteinTech Cat no. 21537-1-AP) (IF 1:100, IB 1:1000), LC3B (Cell Signalling Cat no. 3868S) (IF 1:200, IB 1:1000), p62 (SQSTM1) (Cedarlane Cat no. PM045) (IF 1:200, IB 1:1000), GAPDH (Cell Signalling Cat no. 2118S) (IB 1:1000). HRP conjugated secondary antibodies for immunoblotting were purchased from Thermo Fisher, anti-mouse IgG (H + L) (Cat no. 31430) (1:5000) and anti-rabbit IgG (H + L) (Cat no. 31460) (1:5000). Alexa Fluor tagged secondary antibodies for immunofluorescence were purchased from Thermo Fisher, goat anti-mouse IgG (H + L) 488 (Cat no. A-11029) (1:1000), goat anti-rabbit IgG (H + L) 594 (Cat no. A-11012) (1:500), donkey anti-rabbit IgG (H + L) 647 (Cat no. A31573) (1:500). Hoechst 33342 nuclear stain was purchased from Thermo Fisher (Cat no. H3570) (1:5000).

Cell culture and maintenance: HEK cells, iPSCs/ESCs, and iPSC-derived myoblasts

Human Embryonic Kidney (HEK) wild type and *GNE* knock out cells (a gift from Dr. Rüdiger Horstkorte at Martin Luther University, Halle, Germany)[42] were maintained in 10cm plates in high glucose Dulbecco's Modified Eagle Media (DMEM) (Thermo Fisher Cat no. SH30022FS) supplemented with 10% fetal bovine serum (FBS) (Sigma Cat no. F1051), 1% L-glutamine (Thermo Fisher Cat no. SH3003401), 1% Penicillin-Streptomycin (Fisher Cat no. SV30010) at 37°C, 5% CO_2. Cells were passaged using Trypsin (Thermo Fisher Cat no. 25200072) once they reached 100% confluency.

Human induced pluripotent stem cell (iPSC) and embryonic stem cell (ESC) lines were maintained under feeder-free hypoxic conditions on Matrigel coated plates (Corning Cat no. 40230) in mTeSR Plus (STEMCELL Technologies Cat no. 100–0276) with media changes every other day. Colonies were passaged every 4–6 days using an in-house 0.5mM EDTA solution. The GNEM patient lines were a gift from Drs. Margherita Milone and Jason Doles at the Mayo Clinic, Rochester, USA and the Indiana University School of Medicine, respectively [30]. The PGPC-3 and PGPC-14 control lines were a gift from Dr. James Ellis at Sick Kids, Toronto, Canada [43]. iPSC and ESC lines were differentiated into myogenic progenitors using a serum free differentiation protocol as described in Chal et al [44].

The iPSC-derived myogenic progenitors were cultured on Matrigel coated 6-well plates in Skeletal Muscle Cell Growth Media 2 (Lonza Cat no. CC-3245) at 37°C, 5% CO_2. Cells were passaged using TrypLE (Thermo Fisher Cat no. 12604021) once they reached 50–70% confluency. Both iPSCs, ESCs, and myogenic progenitors were cryopreserved in 90% of their culture media and 10% DMSO.

Cell treatments

For immunoblot experiments HEK cells were seeded at 300,000 cells per well in a 6 well plate. The following evening the media was removed, and fresh glucose and serum free media (Thermo Fisher Cat no. 11966025) was added for the initial 24-hour time point. Media changes were similarly performed for 2-, 4-, 6-, 8-hour time points. An identical time course experiment was performed by replacing media with fresh growth medium containing 25uM of chloroquine (Sigma Cat no. C6628). Following completion of the final time point of the time course, cells were collected as described below.

For immunofluorescence experiments HEK cells were seeded at 2,500 cells/well on Matrigel coated 96-well plates (Ibidi Cat no. 89626-90). Time course experiments were performed as described above. Following the completion of the final time point, cells were washed gently with PBS and fixed for 15 minutes in 4% PFA.

Cell lysate preparation

At experimental end point, cell culture media was removed, and HEK cells were washed with ice cold PBS. Cells were then scraped in 1ml of cold PBS and collected in Eppendorf tubes which were spun down at 1000RPM for 5 minutes at 4°C. The supernatant was removed, and cell pellets were stored at -80°C until lysis. For collection of iPSC-myoblasts, cells were washed with PBS and incubated in TrypLE at 37°C for 5 minutes or until cells detached in single cell suspensions. Cells were then collected in a TrypLE-PBS mixture and spun down at 1000RPM. The supernatant was discarded, and the cell pellets were stored at -80°C until lysis. Cell pellets from both HEK cells and iPSC-myoblasts were then placed on ice, and freshly prepared Triton-X lysis buffer (150mM NaCl, 10mM Tris-HCl, 1x protease and phosphatase inhibitor cocktail, 1% Triton-X) was added to each sample. The pellets were resuspended by pipetting up and down, followed by a brief vortex, and then placed on a rotator at 4°C for 30 minutes. The lysates were subsequently centrifuged at 12,000RPM for 15 minutes at 4°C. The supernatant was transferred to a fresh tube and stored at -80°C while the pellet was discarded.

Immunoblotting

Protein quantification was performed on cell lysates using the DC-Assay (BioRad Cat no. 5000113, 5000114, 5000115) with BSA (Thermo Fisher Cat no. 23209) dilutions as standards. Proteins were resolved by SDS-PAGE and transferred to PVDF membranes. For serglycin immunoblots, proteins were resolved on 10% acrylamide gels and transferred via a wet transfer (25mM tris-base, 190mM glycine, 20% methanol) overnight at 40V at 4°C. For LC3 immunoblots, proteins were resolved on 15% acrylamide gels and transferred using Trans-Blot Turbo Transfer System and Transfer Kit (BioRad Cat no. 1704272). Membranes were incubated with Ponceau S solution (Sigma Cat no. P7170) to ensure proper transfer and equal protein loading. Membranes were then blocked in 4% skim milk in TBST for 1 hour at room temperature. Following blocking, membranes were incubated with primary antibodies of interest at desired dilution overnight at 4°C. Secondary HRP-conjugated antibody incubation was performed for 1 hour at room temperature. Membranes were imaged using Clarity Western ECL (BioRad Cat no. 170–5060) with the ChemiDoc system (BioRad). Immunoblots were quantified using the ImageJ software normalizing the protein of interest either to Ponceau S or loading control GAPDH.

Immunofluorescence

HEK and iPSC-derived myoblasts were grown on Matrigel coated 96-well plates (Ibidi Cat no. 89626-90). Once cells reached the desired confluence or upon completion of previously described time course experiments, cells were washed with PBS and fixed for 15 minutes in 4% PFA. Following fixation cells were washed 3 times with PBS. PFA was quenched in a 0.1M glycine plus 0.1% Triton-X solution for 10 minutes, followed by 3 washes in PBS. Cells were then blocked and permeabilized in a 5% horse serum, 2% BSA, 0.1% Triton-X solution for 30 minutes at room temperature. Following this step cells were incubated with desired primary antibodies in blocking solution without Triton-X overnight at 4°C. The next day cells were washed with PBS and incubated with appropriate secondary fluorescent antibodies for 1 hour in the dark at room temperature. Following additional PBS washes cells were incubated for 10 minutes at room temperature with Hoechst after which they were stored at 4°C in PBS until imaging.

Microscopy

High-throughput imaging was performed on the Revvity Opera Phenix automated confocal system at 63x magnification. Images were analyzed on our Columbus Image Analysis Server using custom pipelines to identify nuclei, spots, and percentage overlap.

Statistical analysis

Data were analyzed using GraphPad Prism version 11.0.1. Statistical comparisons were performed using Welch's t-tests, one-way analysis of variance (ANOVA) with Dunnett's post hoc tests, or mixed-effects two-way ANOVA with Šidák post hoc tests, as appropriate for the experimental design. Results are presented as mean ± standard deviation. Statistical significance was defined as $p < 0.05$. Asterisks indicate levels of significance as follows: *$p < 0.05$, **$p < 0.01$, ***$p < 0.001$, and ****$p < 0.0001$.

Results

Identification of serglycin as potential biomarker in GNEM

As part of a discovery-based approach, unbiased proteomic profiling was performed on serum samples from six patients with GNEM (age range: 35–50 years) and 5 age-matched control individuals using a DIA-based workflow. This analysis enabled the identification of 8 significantly upregulated proteins and 4 significantly downregulated proteins. Among the latter, serglycin was identified based on the quantification of two unique peptides and showed a reduction to 44% of protein abundance compared with control samples (p-value = 0.0001, Fig. 1A, B).

ELISA-based quantification of serglycin was performed to validate the proteomic findings using an independent analytical approach and serum samples derived from further individuals. To this end, a total of 14 serum samples from adult controls (age range: 20–56 years; median age: 34 years) and 23 serum samples from patients with GNEM (age range: 29–57; median age: 41) were analyzed. This analysis revealed a mean serglycin concentration of 4137.76ng/mL in controls and 2684.57ng/mL in GNEM

patient samples, demonstrating a statistically significant reduction of this minimally invasive biomarker in GNEM (t-test $p < 0.0001$, Fig. 1C). Serum serglycin levels showed no significant correlation with age, neither in the overall cohort nor within subgroup analyses. In GNEM patients, age-dependent analysis demonstrated only a weak negative trend ($R^2 = 0.075$; $p = 0.207$), whereas no meaningful association was detectable in controls ($R^2 = 0.002$; $p = 0.924$) (Fig. 1D). Overall, these findings suggest that age does not substantially influence serum serglycin levels and that, at most, GNEM patients may exhibit a trend toward further reduction in association with disease progression.

Characterization of serglycin in cellular models of GNEM

To further validate and characterize serglycin as a candidate biomarker for GNEM, its expression levels were evaluated in cellular models of the disease. The distribution and abundance of serglycin were first examined via immunofluorescence in HEK wild type and *GNE* KO cells. Staining revealed increased intracellular accumulation of serglycin in HEK *GNE* KO cells compared to WT controls (Fig. 2A-C). Serglycin was also assessed by immunoblotting, which detected both the core serglycin protein as well as several higher molecular weight species consistent with its heavily glycosaminoglycan (GAG)-modified forms. These analyses similarly showed increased overall serglycin levels in *GNE* KO cells compared to controls (Fig. 3A-E).

To assess serglycin in a more disease-relevant context, iPSC-derived myoblasts were generated from two GNEM patients and three healthy controls. Immunofluorescence analysis revealed perinuclear localization of serglycin in these cells, consistent with previous reports [40], along with apparent increased intracellular accumulation in both Patient 1 and 2 compared to controls (Fig. 2D-G). Immunoblot analysis showed considerable variability, with no clear trend observed in serglycin levels relative to controls (Fig. 3F-H).

Identification of dysregulated pathways in GNEM

Under the premise that HEK cells in which the *GNE* gene has been knocked out represent a cellular system modelling defective sialic acid homeostasis [42], these cells were used to investigate the effect of GNE protein loss on the global proteomic signature using an unbiased proteomics approach. Consistent with this, the *GNE* knockout cells exhibit a complete absence of polysialic acid (data not shown), supporting their use as a cellular model of GNEM. Based on the known subcellular localization of the GNE protein [45, 46], particular attention was given to proteins residing in the ER-Golgi system, as these are presumed to represent potential targets of primary pathophysiological cascades. The proteomics revealed statistically significant dysregulation of 105 proteins, of which 40 were upregulated and 65 downregulated (Table 1 **and Supplemental Table 1**). Functional annotation of the differentially abundant proteins revealed enrichment of proteins involved in secretory pathway and membrane trafficking processes. Among the highlighted proteins, multiple components of the ER-Golgi glycosylation machinery and nucleotide-sugar transport system were identified, including TMEM165, SLC35B2, SLC35E1, POFUT1, GALNT2, and the lysosomal sialidase NEU1, pointing to perturbations in glycosylation processes. In addition, several proteins associated with Golgi organization and vesicular

trafficking were dysregulated, such as GLG1, GOLIM4, ARFGAP3, ASPSCR1, STK26, LRRC59, JAGN1 and SPAG9. Notably, a substantial subset of proteins participate in endosomal and lysosomal transport pathways, including TM9SF1, STX7, SMAP2, RAB9A, VAMP7, TBC1D23, and SPG21, suggesting broader alterations of the cellular protein clearance machinery. Along this line, proteins linked to autophagy and proteostasis, such as SQSTM1/p62 and SNCA, were also affected. Finally, changes were observed in ER-Golgi resident enzymes involved in lipid metabolism and membrane homeostasis (SPTLC2, ACSL1, ACSL4, CRAT), processes that are critical for vesicle formation and organelle integrity.

Table 1

Key proteins up- or downregulated in HEK GNE knockout cells compared with wildtype. Proteins with p-value of ≤ 0.05 and an abundance ratio (denoted as fold change) of either ≥ 2 (upregulated) or ≤ 0.5 (down-regulated) are included in this table.

Gene	Description	Possible Function	Fold Change
TM9SF1	Transmembrane 9 superfamily member 1	Endosomal-lysosomal trafficking	9.44
TMEM165	Transmembrane protein 165	Golgi membrane protein involved in Mn^{2+} homeostasis and glycosylation	3.71
SLC35B2	Adenosine 3'-phospho 5'-phosphosulfate transporter 1	Golgi 3'-phosphoadenylyl sulfate:adenosine 3',5'-bisphosphate transporter for sulfation reactions	3.26
SLC35E1	Solute carrier family 35 member E1	Nucleotide sugar transporter (Golgi-associated)	2.61
SQSTM1	Sequestosome-1	Selective autophagy receptor (p62); ubiquitin-binding scaffold	2.54
POFUT1	GDP-fucose protein O-fucosyltransferase 1	ER glycosyltransferase O-Fuc family	2.45
SNCA	Alpha-synuclein	Alpha-synuclein; synaptic vesicle regulation	2.43
GLG1	Golgi apparatus protein 1	Golgi glycoprotein; cargo trafficking receptor	2.39
GOLIM4	Golgi integral membrane protein 4	Golgi integral membrane protein; vesicle trafficking	2.36
ARFGAP3	ADP-ribosylation factor GTPase-activating protein 3	ARF1 GTPase-activating protein; COPI vesicle formation	2.33
GALNT2	Polypeptide N-acetylgalactosaminyltransferase 2	Golgi O-glycosyltransferase initiating mucin-type glycosylation	2.18
ASPSCR1	Tether containing UBX domain for GLUT4	Tethering protein for GLUT4 vesicles	2.15
STX7	Syntaxin-7	Endosomal SNARE protein mediating late endosome–lysosome fusion	2.15
SMAP2	Stromal membrane-associated protein 2	Role in clathrin-dependent retrograde transport from early endosomes to trans-Golgi network	2.14
NEU1	Sialidase-1	Lysosomal sialidase; glycoprotein degradation	2.09

Gene	Description	Possible Function	Fold Change
JAGN1	Protein jagunal homolog 1	Endoplasmic reticulum transmembrane protein involved in vesicle-mediated transport	0.48
RAB9A	Ras-related protein Rab-9A	Late endosome-to-Golgi trafficking GTPase	0.43
SPG21	Maspardin	Endosomal-lysosomal trafficking protein	0.40
STK26	Serine/threonine-protein kinase 26	Serine/threonine kinase; Golgi polarization & exocytosis	0.40
VAMP7	Vesicle-associated membrane protein 7	Vesicular SNARE; late endosome/lysosome fusion	0.40
TBC1D23	TBC1 domain family member 23	Endosome-to-Golgi trafficking	0.38
LRRC59	Leucine-rich repeat-containing protein 59	ER membrane ribosome receptor; nuclear import modulation	0.22
ATP11C	Phospholipid-transporting ATPase IG	Phospholipid flippase; vesicle membrane asymmetry	0.18

Taken together, these findings reveal that loss of GNE is associated with coordinated alterations in proteins regulating glycosylation, ER-Golgi organization, and endosomal-lysosomal trafficking, suggesting that disruption of the secretory and membrane trafficking systems may represent an important downstream consequence of impaired sialic acid homeostasis.

Dysfunctional autophagic flux in GNE KO cells

Rimmed vacuoles containing protein aggregates are a hallmark feature observed in muscle biopsies from GNEM patients [47, 48]. These biopsies stain positive for autophagy-associated markers including LC3 and p62/SQSTM1, supporting a possible connection between disrupted autophagy and rimmed vacuole formation [4, 30, 35, 48, 49]. Consistent with this, multiple studies have reported impaired autophagic flux across various cellular models of GNEM [30, 32, 33]. Autophagic flux was therefore examined in HEK WT and *GNE* KO cells lines motivated in part by prior proteomics data (Table 1) which showed increased abundance of p62/SQSTM1 in *GNE* KO relative to WT cells, a finding which was further validated by immunoblot analysis (Fig. 4).

Immunofluorescence studies were also conducted in the HEK cells following chloroquine (CQ) treatment, an autophagy inhibitor that blocks autophagosome-lysosome fusion, as well as under glucose and serum free conditions (GF) which induces cellular stress and autophagy. Initial experiments demonstrated an increase in p62 staining in HEK *GNE* KO cells compared to controls across all time points ($p = 0.038$), while LC3 staining exhibited greater variability but overall tended to be lower in the *GNE* KO cells relative to WT ($p = 0.0846$) (Fig. 5).

A parallel time-course analysis using immunoblotting assessed the LC3II/I ratio, a commonly used read out for autophagic flux, following either CQ treatment or GF media starvation. Significant differences were observed between wildtype and *GNE* KO cells under both treatment conditions ($p < 0.05$ for CQ and GF), with *GNE* KO cells exhibiting a blunted response. These findings are consistent with a potential defect in autophagosome maturation and/or lysosomal clearance in the *GNE* KO cells (Fig. 6).

Serglycin accumulates in lysosomal and ER-Phagy compartments in GNEM myoblasts

To further investigate whether serglycin accumulation is linked to defects in autophagy-related degradation pathways, its subcellular localization was assessed relative to lysosomal and ER-phagy markers. iPSC-derived myoblasts, which exhibit prominent perinuclear serglycin staining, were used for overlap analysis with the lysosome marker LAMP1, and ER-phagy marker FAM134B. Initial experiments showed increased overlap between serglycin and LAMP1 in Patient 2 compared to control (Fig. 7), while enhanced overlap with FAM134B was evident in both patients lines relative to controls (Fig. 8). These findings are consistent with the possibility that retained serglycin is directed to lysosomal and ER-phagy compartments for degradation, a process that may be impaired in the context of autophagic dysfunction.

Discussion

In this study, serglycin was identified as a dysregulated proteoglycan in both patient serum and cellular models of GNEM, supporting its potential utility as a candidate disease biomarker. The data are consistent with a model in which serglycin accumulation may arise from impaired secretion coupled with defective autophagic and lysosomal processing. These findings suggest that GNE deficiency may be associated with disruption of key proteins involved in vesicle trafficking and exocytosis, which may contribute to the intracellular retention of serglycin and its rerouting to dysfunctional degradative pathways. Overall, this study extends the current understanding of GNEM pathogenesis and supports serglycin as a candidate circulating biomarker.

Consistent with this interpretation, intracellular accumulation of serglycin was observed across multiple cellular models, including HEK *GNE* knockout cells and iPSC-derived GNEM patient myoblasts. Serglycin in iPSC-derived myoblasts localized predominantly to the perinuclear region, consistent with prior reports describing its enrichment within cytoplasmic vesicles and reliance on the classical secretory pathway for secretion [40]. Importantly, these cellular observations are concordant with the serum proteomics and ELISA data demonstrating reduced circulating serglycin in GNEM patients, consistent with the possibility that serglycin is synthesized and post-translationally modified but may not be efficiently secreted.

Importantly, no detectable changes in the molecular weight or banding patterns of serglycin were observed by immunoblot, suggesting no major changes in core protein size or gross glycosaminoglycan (GAG) modifications. This is consistent with the known biology of serglycin, which is predominantly

modified by sulfated GAG chains rather than N- or O-linked glycans terminating in sialic acid [38, 39, 50]. As such, its dysregulation is unlikely to reflect defective biosynthesis or glycan modification but may instead point toward abnormalities in its intracellular trafficking, secretion, or degradation.

These observations are consistent with a model where defective secretion may represent an early event in serglycin dysregulation, alongside broader disruptions in autophagy and proteostasis. Inhibition of ER-to-Golgi transport has previously been shown to result in intracellular retention of serglycin in myoblasts [40], which is consistent with the possibility that defects in vesicle transport or exocytosis could contribute to its accumulation within perinuclear compartments. In this context, serglycin may be redirected towards autophagic-lysosomal pathways for clearance however, defects in these pathways could limit efficient degradation potentially contributing to its intracellular buildup.

Proteomic profiling of HEK wildtype and *GNE* knockout cells are consistent with this perturbed trafficking model by showing widespread alterations in proteins associated with the secretory pathway, including components involved in ER-Golgi trafficking, Golgi organization, glycosylation machinery, and endosomal-lysosomal transport. In addition, dysregulation of proteins involved autophagy, proteostasis, and lipid metabolism were also observed. Collectively, these findings suggest that loss of GNE is accompanied by coordinated perturbations across multiple interconnected pathways governing secretory trafficking and cellular protein handling. These findings also suggest that disruption of ER-Golgi and endosomal-lysosomal systems represents an important downstream consequence of GNE dysfunction.

Consistent with previous reports, autophagic dysfunction was observed in the HEK *GNE* KO cells as indicated by increased p62 accumulation and a blunted LC3-II/I response following both nutrient deprivation and chloroquine treatment. These findings align with prior studies in GNEM models, which collectively suggest defects across multiple stages of the autophagy-lysosome pathway [30, 31, 33–36, 51, 52]. Supporting this, the increased overlap of serglycin with LAMP1-positive lysosomal compartments and the ER-phagy receptor FAM134B in GNEM patient iPSC-derived myoblasts suggests that the retained serglycin may be redirected toward autophagic-lysosomal and ER-associated degradative pathways. In the setting of compromised degradative function, this rerouting may be insufficient to result in efficient clearance, instead further contributing to the observed intracellular accumulation of serglycin in GNEM cells.

Several limitations of this study warrant consideration. While the data are consistent with impaired secretion and autophagic handling of serglycin, direct assessment of vesicle trafficking dynamics was not performed and will be important to address in future studies. Additionally, it remains unclear whether serglycin accumulation contributes to muscle pathology or primarily reflects broader cellular dysfunction associated with GNEM. Further, given that defects in autophagy have been observed in other myopathies, the specificity of serglycin dysregulation to GNEM remains to be established. More broadly, while the proposed model is supported by correlative evidence, further studies will be required to

determine causal relationships between *GNE* mutations, trafficking alterations, and serglycin accumulation.

From a clinical perspective, the consistent reduction of serglycin in patient serum, and its intracellular accumulation in disease relevant cellular models, suggest its potential as a minimally invasive candidate biomarker for GNEM. Serglycin may be useful in patient stratification, monitoring disease progression, or assessing therapeutic response, particularly for interventions targeting sialylation, cellular trafficking, or autophagic pathways. However, further validation in larger, well-characterized clinical cohorts is required, along with additional assessments of disease specificity, longitudinal dynamics and reproducibility across multiple detection platforms.

In summary, these findings suggest that serglycin lies at the intersection of defective secretion, and impaired autophagy in GNEM. Disruption of vesicle trafficking and exocytosis may contribute to the intracellular retention and misdirection of serglycin toward dysfunctional degradative pathways. This work provides additional insights into the current understanding of GNEM pathogenesis and highlights serglycin as a preliminary candidate biomarker reflecting broader defects in cellular trafficking and proteostasis.

Declarations

Ethics approval and consent to participate

Transfer of GNE myopathy patient iPSCs to University of Ottawa/CHEO Research Institute approved by Mayo Clinic Biospecimen Subcommittee on April 7, 2023 and Mayo Clinic IRB on May 26, 2023.

Consent for publication

Not applicable.

Funding

HL receives support from the Canadian Institutes of Health Research (CIHR) for Foundation Grant FDN-167281 (Precision Health for Neuromuscular Diseases), Transnational Team Grant ERT-174211 (ProDGNE) and Network Grant OR2-189333 (NMD4C), from the Canada Foundation for Innovation (CFI-JELF 38412), the Canada Research Chairs program (Canada Research Chair in Neuromuscular Genomics and Health, 950-232279), the European Commission (Grant # 101080249) and the Canada Research Coordinating Committee New Frontiers in Research Fund (NFRFG-2022-00033) for SIMPATHIC, and from the Government of Canada Canada First Research Excellence Fund (CFREF) for the Brain-Heart Interconnectome (CFREF-2022-00007). AD holds a Canadian Institutes of Health Research (CIHR) Canada Graduate Scholarship Doctoral (CGS-D) award (494291). AH acknowledges the support by the “Ministerium für Kultur und Wissenschaft des Landes Nordrhein-Westfalen” and “Der Regierende

Bürgermeister von Berlin, Senatskanzlei Wissenschaft und Forschung” and the Bundesministerium für Forschung, Technologie und Raumfahrt (BMFTR). MM receives funding from the MDA award ID: 497263.

Author Contribution

Conceptualization was carried out by A.D., V.D., A.H., S.H.H., L.C., S.S., A.R., and H.L. Methodology was developed by A.D., V.D., A.H., and T.R. Analysis was performed by A.D., V.D., A.H., and A.R. Investigations were conducted by A.D., V.D., A.H., and S.B. Resources were provided by A.H., T.R., R.H., J.D.D., M.M., S.S., A.R., and H.L. The original draft of the manuscript was written by A.D., A.H., and A.R. Revisions and editing of the manuscript were performed by A.D., S.S., A.R., and H.L. Visualization was carried out by A.D., V.D., A.H., S.S., A.R., and H.L. Project administration was managed by S.S., A.R., and H.L. Funding acquisition was handled by A.D., S.S., and H.L. All authors have read, provided feedback on, and agreed to the final version of this manuscript.

Acknowledgement

Thank you to Dr. James Ellis (Sick Kids, Toronto, Canada) for two control iPSC lines (PGPC3 and PGPC14). We would also like to thank Dr. Rita Gerardy-Schahn (Hannover, Germany) for supplying the PolySia 735 antibody.

Data Availability

Processed proteomics data generated during this study are available in the Supplementary Materials accompanying this article.

References

1. Eisenberg I, Avidan N, Potikha T, Hochner H, Chen M, Olender T et al (2001) The UDP-N-acetylglucosamine 2-epimerase/N-acetylmannosamine kinase gene is mutated in recessive hereditary inclusion body myopathy. Nat Genet 29:83–87. https://doi.org/10.1038/ng718
2. Hinderlich S, Stasche R, Zeitler R, Reutter W (1997) A bifunctional enzyme catalyzes the first two steps in N-acetylneuraminic acid biosynthesis of rat liver. Purification and characterization of UDP-N-acetylglucosamine 2-epimerase/N-acetylmannosamine kinase. J Biol Chem 272:24313–24318. https://doi.org/10.1074/jbc.272.39.24313. 1997/09/26 ed
3. Huizing M, Carrillo-Carrasco N, Malicdan MCV, Noguchi S, Gahl WA, Mitrani-Rosenbaum S et al (2014) GNE myopathy: New name and new mutation nomenclature. Neuromuscul Disord Elsevier Ltd 24:387–389. https://doi.org/10.1016/j.nmd.2014.03.004
4. Pogoryelova O, Gonzalez Coraspe JA, Nikolenko N, Lochmuller H, Roos A (2018) GNE myopathy: from clinics and genetics to pathology and research strategies. Orphanet J Rare Dis 13:70.

https://doi.org/10.1186/s13023-018-0802-x. 2018/05/04 ed

5. Saito F, Tomimitsu H, Arai K, Nakai S, Kanda T, Shimizu T et al (2004) A Japanese patient with distal myopathy with rimmed vacuoles: Missense mutations in the epimerase domain of the UDP-N-acetylglucosamine 2-epimerase/N-acetylmannosamine kinase (GNE) gene accompanied by hyposialylation of skeletal muscle glycoproteins. Neuromuscul Disord 14:158–161. https://doi.org/10.1016/j.nmd.2003.09.006
6. Voermans NC, Guillard M, Doedee R, Lammens M, Huizing M, Padberg GW et al (2010) Clinical features, lectin staining, and a novel GNE frameshift mutation in hereditary inclusion body myopathy. Clin Neuropathol. /02/24 ed. 2010;29:71–7
7. Leoyklang P, Malicdan MC, Yardeni T, Celeste F, Ciccone C, Li X et al (2014) Sialylation of Thomsen-Friedenreich antigen is a noninvasive blood-based biomarker for GNE myopathy. Biomarkers Med 8:641–652. https://doi.org/10.2217/bmm.14.2
8. Lochmuller H, Behin A, Caraco Y, Lau H, Mirabella M, Tournev I et al (2019) A phase 3 randomized study evaluating sialic acid extended-release for GNE myopathy. Neurology. 2019/05/01. 92:e2109–e2117. https://doi.org/10.1212/WNL.0000000000006932
9. Go H, Sung NJ, Choi J, Kim L, Park EJ (2024) 6'-sialyllactose prevents dexamethasone-induced muscle atrophy by controlling the muscle protein degradation pathway. Biochem Biophys Res Commun 736:150892. https://doi.org/10.1016/j.bbrc.2024.150892
10. Mori-Yoshimura M, Suzuki N, Katsuno M, Takahashi MP, Yamashita S, Oya Y et al (2023) Efficacy confirmation study of aceneuramic acid administration for GNE myopathy in Japan. Orphanet J Rare Dis 18:241. https://doi.org/10.1186/s13023-023-02850-y
11. Park Y-E, Park E, Choi J, Go H, Park DB, Kim M-Y et al (2023) Pharmacokinetics and clinical efficacy of 6'-sialyllactose in patients with GNE myopathy: Randomized pilot trial. Biomed Pharmacother 168:115689. https://doi.org/10.1016/j.biopha.2023.115689
12. Carrillo N, Malicdan MC, Leoyklang P, Shrader JA, Joe G, Slota C et al (2021) Safety and efficacy of N-acetylmannosamine (ManNAc) in patients with GNE myopathy: an open-label phase 2 study. Gen Med United States: Springer Nat 23:2067–2075. https://doi.org/10.1038/s41436-021-01259-x
13. Mullen J, Alrasheed K, Mozaffar T (2022) GNE myopathy: History, etiology, and treatment trials. Front Neurol 18:1002310. https://doi.org/10.3389/fneur.2022.1002310
14. Das T, Das S, Das SRC, Ghose S, Das A, Chowdhury S et al (2025) Integrating multimodal biomarker strategies: A narrative review of molecular and characteristic imaging techniques for better monitoring of neurodegenerative diseases. NeuroMarkers 100131. https://doi.org/10.1016/j.neumar.2025.100131
15. Bodaghi A, Fattahi N, Ramazani A, Biomarkers (2023) Promising and valuable tools towards diagnosis, prognosis and treatment of Covid-19 and other diseases. Heliyon 9:e13323. https://doi.org/10.1016/j.heliyon.2023.e13323
16. Ferlini A, Scotton C, Novelli G (2013) Biomarkers in rare diseases. Public Health Genomics 16:313–321. https://doi.org/10.1159/000355938

17. Pereira BL, Barbosa M, Granjo P, Lochmüller H, Videira PA (2025) Beyond sialylation: Exploring the multifaceted role of GNE in GNE myopathy. Mol Genet Metab 144:109075. https://doi.org/10.1016/j.ymgme.2025.109075
18. Weidemann W, Stelzl U, Lisewski U, Bork K, Wanker EE, Hinderlich S et al (2006) The collapsin response mediator protein 1 (CRMP-1) and the promyelocytic leukemia zinc finger protein (PLZF) bind to UDP-N-acetylglucosamine 2-epimerase/N-acetylmannosamine kinase (GNE), the key enzyme of sialic acid biosynthesis. FEBS Lett 580:6649–6654. https://doi.org/10.1016/j.febslet.2006.11.015
19. Devi SS, Yadav R, Arya R (2021) Altered Actin Dynamics in Cell Migration of GNE Mutant Cells. Front Cell Dev Biol. /04/06 ed. 2021;9:603742. https://doi.org/10.3389/fcell.2021.603742
20. Yadav R, Oswalia J, Ghosh A, Arya R (2022) Effect of GNE Mutations on Cytoskeletal Network Proteins: Potential Gateway to Understand Pathomechanism of GNEM. Neuromolecular Med. https://doi.org/10.1007/s12017-022-08711-4
21. Devi SS, Arya R (2017) Effect of altering sialylation levels on cytoskeletal organization of the cell. Mol Biol Cell Am Soc Cell Biology 28. https://doi.org/10.1091/mbc.E17-10-0618
22. Sela I, Krentsis IM, Shlomai Z, Sadeh M, Dabby R, Argov Z et al (2011) The proteomic profile of hereditary inclusion body myopathy. PLoS ONE United States 6:e16334. https://doi.org/10.1371/journal.pone.0016334
23. Amsili S, Zer H, Hinderlich S, Krause S, Becker-Cohen M, MacArthur DG et al (2008) UDP-N-acetylglucosamine 2-epimerase/N-acetylmannosamine kinase (GNE) binds to alpha-actinin 1: novel pathways in skeletal muscle? PLoS ONE 3:e2477. https://doi.org/10.1371/journal.pone.0002477. 2008/06/19 ed
24. Cho A, Christine M, Malicdan V, Miyakawa M, Nonaka I, Nishino I et al (2017) Sialic acid deficiency is associated with oxidative stress leading to muscle atrophy and weakness in GNE myopathy. Hum Mol Genet 26:3081–3093. https://doi.org/10.1093/hmg/ddx192
25. Cho A, Malicdan MC, Nonaka I, Hayashi YK, Nishino I, Noguchi S (2012) Muscle atrophy in the GNE myopathy mouse model is associated with oxidative stress. Neuromuscul Disord Elsevier Ltd 22:816. https://doi.org/10.1016/j.nmd.2012.06.049
26. Chaudhary P, Sharma S, Singh R, Arya R (2021) Elucidation of ER stress and UPR pathway in sialic acid-deficient cells: Pathological relevance to GNEM. J Cell Biochem. /09/24 ed. 2021;122:1886–902. https://doi.org/10.1002/jcb.30148
27. Li H, Chen Q, Liu F, Zhang X, Li W, Liu S et al (2013) Unfolded Protein Response and Activated Degradative Pathways Regulation in GNE Myopathy. PLoS ONE United States 8:e58116. https://doi.org/10.1371/journal.pone.0058116
28. Devi S, Yadav R, Chanana P, Arya R (2018) Fighting the cause of Alzheimer's and GNE myopathy. Front Neurosci 15:669. https://doi.org/10.3389/fnins.2018.00669
29. Yadav R, Devi SS, Oswalia J, Ramalingam S, Arya R (2022) Role of HSP70 chaperone in protein aggregate phenomenon of GNE mutant cells: Therapeutic lead for GNE Myopathy. Int J Biochem Cell Biol 149:106258. https://doi.org/10.1016/j.biocel.2022.106258

30. Schmitt RE, Smith DY, Cho DS, Kirkeby LA, Resch ZT, Liewluck T et al (2022) Myogenesis defects in a patient-derived iPSC model of hereditary GNE myopathy. npj Regen Med 7:1–17. https://doi.org/10.1038/s41536-022-00238-3
31. Zhang T, Yin X, Yu X, Shang R, Lu L, Miao J (2023) Metformin protects fibroblasts from patients with GNE myopathy by restoring autophagic flux via an AMPK/mTOR-independent pathway. Biomed Pharmacother 164:114958. https://doi.org/10.1016/j.biopha.2023.114958
32. Oswalia J, Singh S, Gautam V, Arya R (2024) Altered autophagic flux in GNE mutant cells of Indian origin: Potential drug target for GNE myopathy. Exp Cell Res 440:114118. https://doi.org/10.1016/j.yexcr.2024.114118
33. Kim D-W, Kwon E-J, Kwon H, Kim J, Cha H-J (2026) Defective autophagy in GNE myopathy is rescued by inhibition of noncanonical Akt–mTORC1 activation across multiple isogenic models. Exp Mol Med Nat Publishing Group 1–16. https://doi.org/10.1038/s12276-026-01701-7
34. Murakami N, Ihara Y, Nonaka I (1995) Muscle fiber degeneration in distal myopathy with rimmed vacuole formation. Acta Neuropathol 89:29–34. https://doi.org/10.1007/BF00294256
35. Papadimas GK, Evila A, Papadopoulos C, Kararizou E, Manta P, Udd B (2016) GNE-Myopathy in a Greek Romani Family with Unusual Calf Phenotype and Protein Aggregation Pathology. J Neuromusc Dis 3:283–288. https://doi.org/10.3233/JND-160154
36. Tsuruta Y, Furuta A, Furuta K, Yamada T, Kira J, Iwaki T (2001) Expression of the lysosome-associated membrane proteins in myopathies with rimmed vacuoles. Acta Neuropathol 101:579–584. https://doi.org/10.1007/s004010000329
37. Sharma S, Mashangva F, Oswalia J, Singh S, Alag R, Arya R (2024) Calcium level and autophagy defect in GNE mutants of rare neuromuscular disorder. Cell Biol Int 49:343–356. https://doi.org/10.1002/cbin.12268
38. Scully OJ, Chua P-J, Harve KS, Bay B-H, Yip GW (2012) Serglycin in Health and Diseases. Anat Rec 295:1415–1420. https://doi.org/10.1002/ar.22536
39. Kolset SO, Tveit H (2008) Serglycin – Structure and biology. Cell Mol Life Sci 65:1073–1085. https://doi.org/10.1007/s00018-007-7455-6
40. Hjorth M, Norheim F, Meen AJ, Shirin P, Sindre L, Torgeir H et al (2015) The effect of acute and long-term physical activity on extracellular matrix and serglycin in human skeletal muscle. Physiological Rep Physiol Rep 3. https://doi.org/10.14814/phy2.12473
41. Burkhart JM, Schumbrutzki C, Wortelkamp S, Sickmann A, Zahedi RP (2012) Systematic and quantitative comparison of digest efficiency and specificity reveals the impact of trypsin quality on MS-based proteomics. J Proteom 75:1454–1462. https://doi.org/10.1016/j.jprot.2011.11.016
42. Peters E, Selke P, Bork K, Horstkorte R, Gesper A (2023) Evaluation of N-Acetylmannosamine Administration to Restore Sialylation in GNE-Deficient Human Embryonal Kidney Cells. Front Biosci (Landmark Ed). Landmark Ed 28:300. https://doi.org/10.31083/j.fbl2811300
43. Hildebrandt MR, Reuter MS, Wei W, Tayebi N, Liu J, Sharmin S et al (2019) Precision Health Resource of Control iPSC Lines for Versatile Multilineage Differentiation. Stem Cell Rep 13:1126–1141.

https://doi.org/10.1016/j.stemcr.2019.11.003

44. Chal J, Al Tanoury Z, Hestin M, Gobert B, Aivio S, Hick A et al (2016) Generation of human muscle fibers and satellite-like cells from human pluripotent stem cells in vitro. Nat Protoc Nat Publishing Group 11:1833–1850. https://doi.org/10.1038/nprot.2016.110
45. Krause S, Hinderlich S, Amsili S, Horstkorte R, Wiendl H, Argov Z et al (2005) Localization of UDP-GlcNAc 2-epimerase/ManAc kinase (GNE) in the Golgi complex and the nucleus of mammalian cells. Exp Cell Res 304:365–379. https://doi.org/10.1016/j.yexcr.2004.11.010. 2005/03/08 ed
46. Krause S, Aleo A, Hinderlich S, Merlini L, Tournev I, Walter MC et al (2007) GNE protein expression and subcellular distribution are unaltered in HIBM. Neurology 69:655–659. https://doi.org/10.1212/01.wnl.0000267426.97138.fd
47. Carrillo N, Malicdan MC, Huizing MGNE, Myopathy (2018) Etiology, Diagnosis, and Therapeutic Challenges. Neurotherapeutics. /10/20 ed. 2018;15:900–14. https://doi.org/10.1007/s13311-018-0671-y
48. Nishino I, Carrillo-Carrasco N, Argov Z (2015) GNE myopathy: Current update and future therapy. J Neurol Neurosurg Psychiatry 86:385–392. https://doi.org/10.1136/jnnp-2013-307051
49. Nonaka I, Noguchi S, Nishino I (2005) Distal myopathy with rimmed vacuoles and hereditary inclusion body myopathy. Curr Neurol Neurosci Rep 5:61–65. https://doi.org/10.1007/s11910-005-0025-0
50. Korpetinou A, Skandalis SS, Labropoulou VT, Smirlaki G, Noulas A, Karamanos NK et al (2014) Serglycin: At the Crossroad of Inflammation and Malignancy. Front Oncol 3:327. https://doi.org/10.3389/fonc.2013.00327
51. Malicdan MCV, Noguchi S, Nonaka I, Hayashi YK, Nishino I, Erratum (2007) A Gne knockout mouse expressing human V572L mutation develops features similar to distal myopathy with rimmed vacuoles or hereditary inclusion body myopathy (Human Molecular Genetics vol. 16 115–128) 10.1093/hmg/ddl446). Human Molecular Genetics. 2007;16:2647. https://doi.org/10.1093/hmg/ddm231
52. Zhang T, Shang R, Miao J (2022) The role of amyloid β in the pathological mechanism of GNE myopathy. Neurol Sci 43:6309–6321. https://doi.org/10.1007/s10072-022-06301-7

Figures

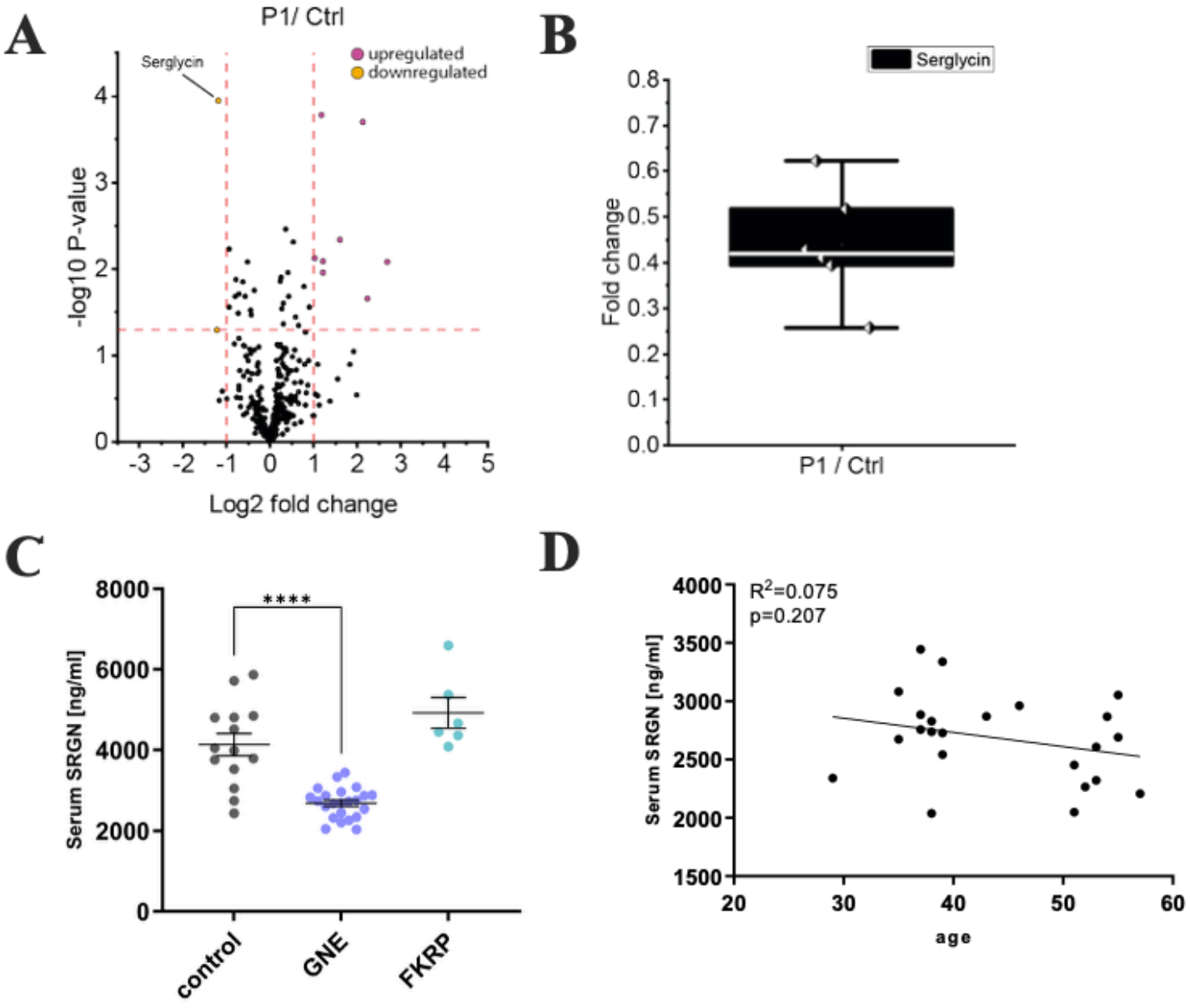


Figure 1

Identification and validation of serglycin as a serum biomarker in GNE myopathy.

A) Volcano plot of DIA-based serum proteomics data comparing a GNEM patient compared to control
B) Box plot of serum proteomics findings showing reduced serglycin abundance in a GNEM patient relative to control.

C) ELISA-based quantification demonstrating reduced serglycin levels in GNEM patients compared with healthy controls and FKRP-associated muscular dystrophy-dystroglycanopathy patients.

D) Correlation analysis of serum serglycin concentration and age in GNEM patients

P1: Patient 1; Ctrl: Control; SRGN: serglycin.

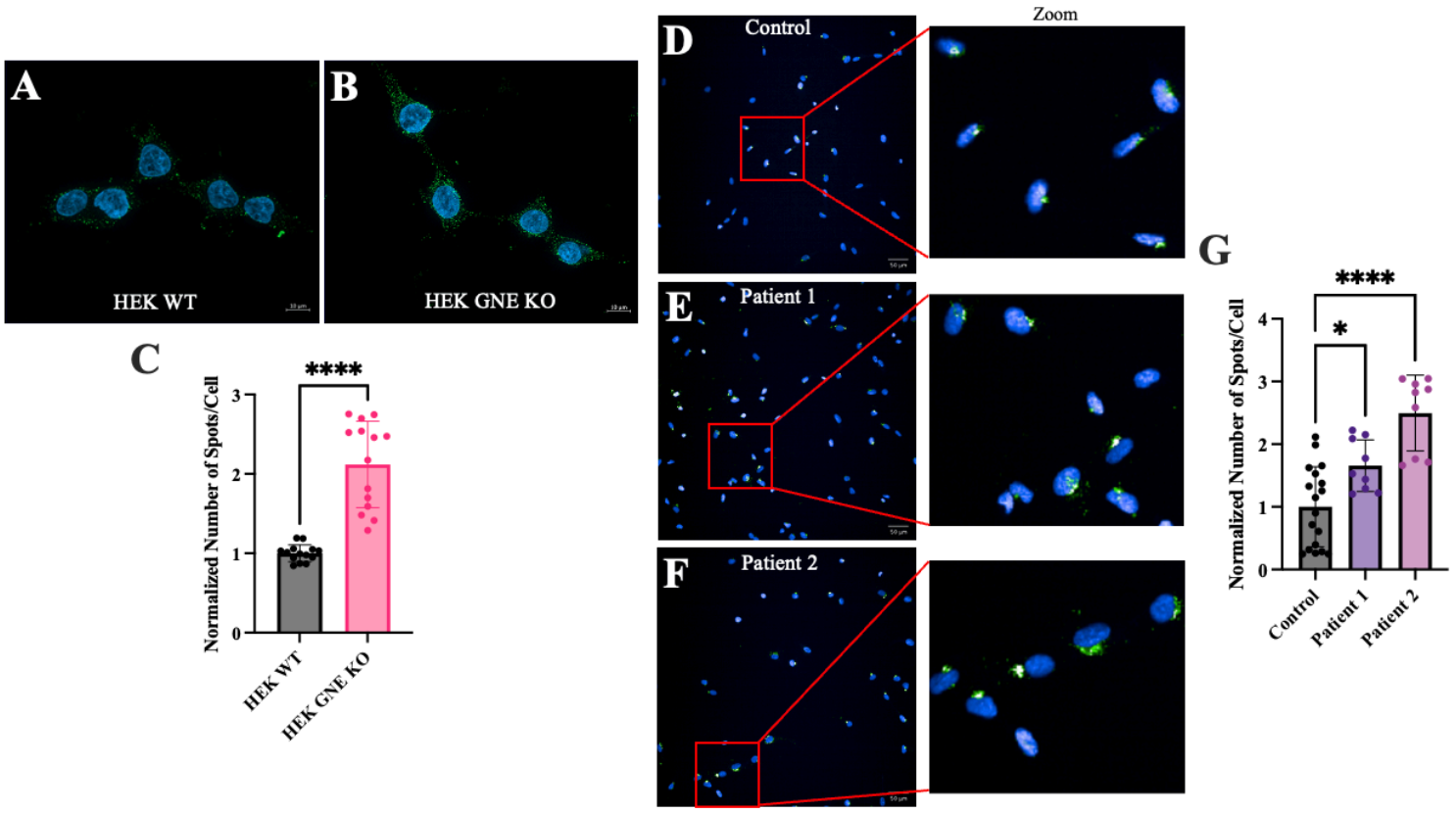


Figure 2

Immunofluorescence analysis and quantification of serglycin in cellular models of GNE myopathy.
A-B) Representative serglycin staining in HEK WT (A) and *GNE* KO (B) cells (green = serglycin, blue = Hoechst).
C) Quantification of serglycin puncta in HEK WT and *GNE* KO cells, showing increased puncta in *GNE* KO (n=14 wells (approx. 2000 cells/well) across 3 plates).
D–F) Representative perinuclear serglycin staining in iPSC-derived myoblasts from a control (D) and GNEM patients 1 (E) and 2 (F). Red boxes indicate regions shown at higher magnification on the right.
G) Quantification of serglycin puncta in iPSC-derived myoblasts from controls and GNEM patients (n=9-18 wells (approx. 1000 cells/well) across 3 plates; two control lines combined into one bar).

SRGN: serglycin. Scale Bar 10um (HEK cells) and 50um (iPSC-myoblasts).

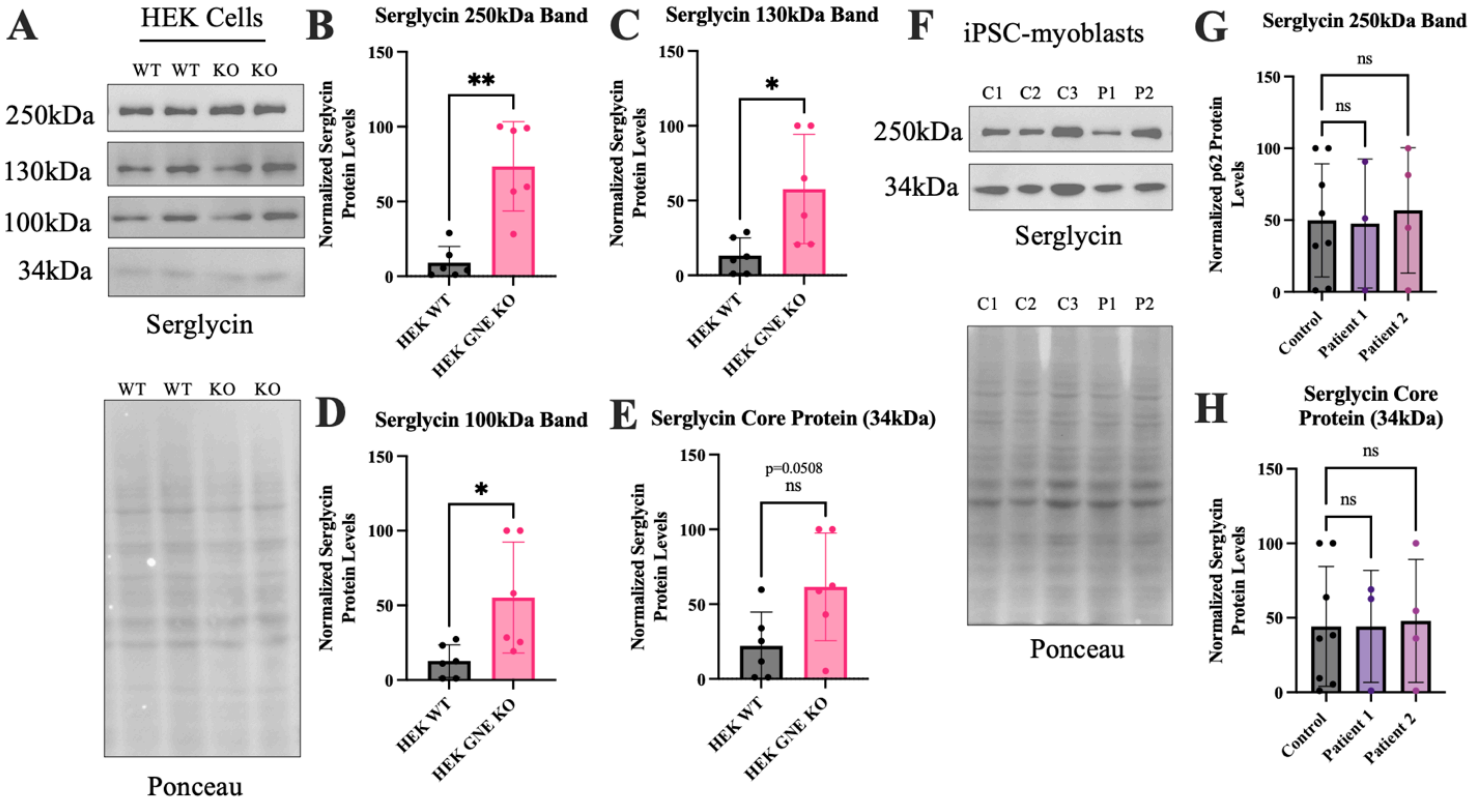


Figure 3

Immunoblot analysis and quantification of serglycin in cellular models of GNE myopathy.

A) Representative serglycin immunoblot in HEK WT and *GNE* KO cells.

B-E) Quantification of distinct serglycin bands from HEK WT and *GNE* KO immunoblots (n=6)

F) Representative serglycin immunoblot in iPSC-derived myoblasts from controls (C) and GNEM patients (Pt).

G-H) Quantification of distinct serglycin bands from iPSC-derived myoblasts (n=2-4; three control lines are plotted within the control bar).

WT = HEK wildtype; KO = HEK GNE knockout; C = control; Pt = patient.

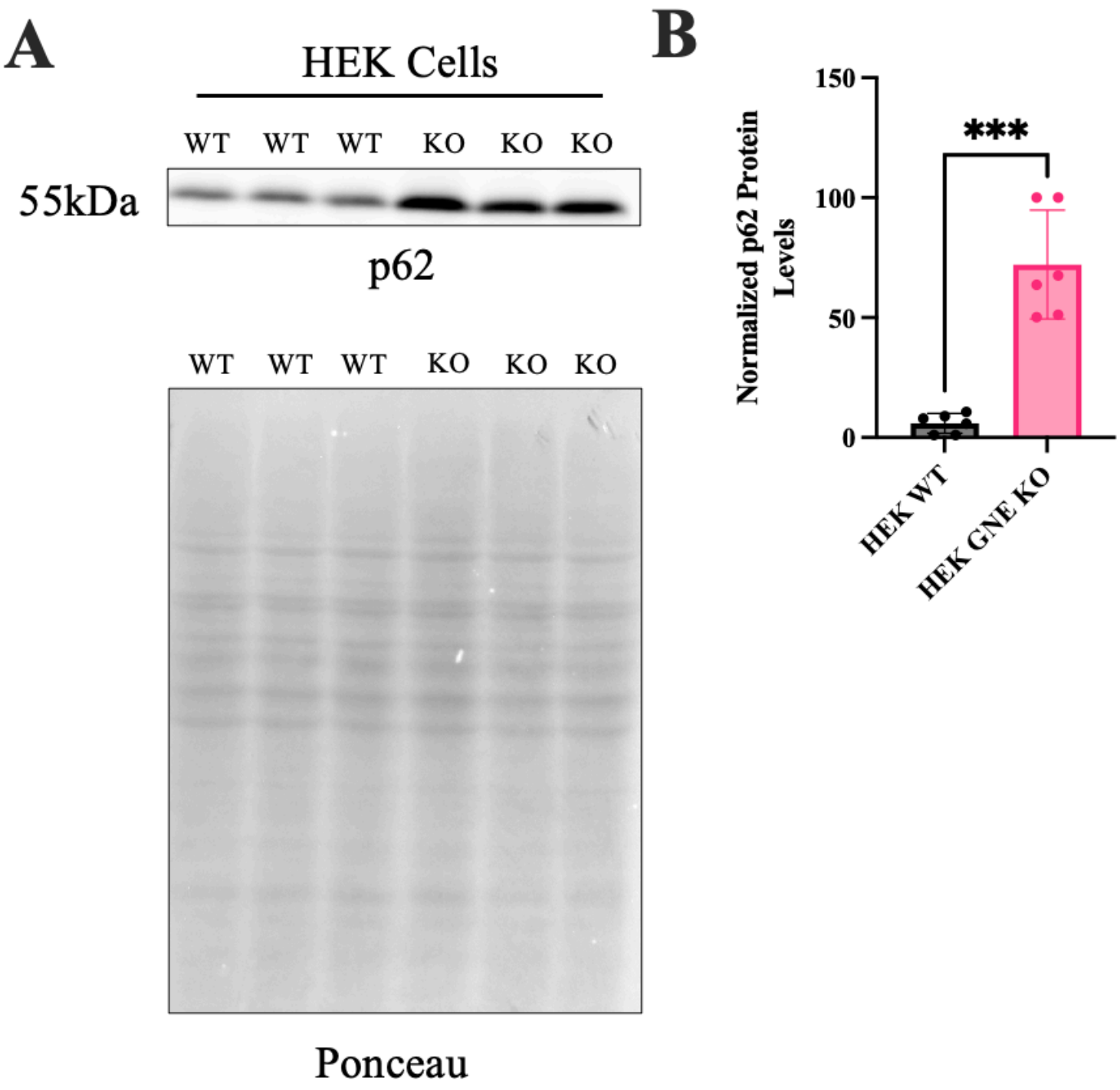


Figure 4

Immunoblot analysis and quantification of p62 via cellular models of GNE Myopathy.

A) Serglycin immunoblot in HEK wildtype and *GNE* knockout cells.

B) Quantification of p62 on immunoblot from HEK WT and *GNE* KO cells (n=6)

WT = HEK wildtype; KO = HEK GNE knockout.

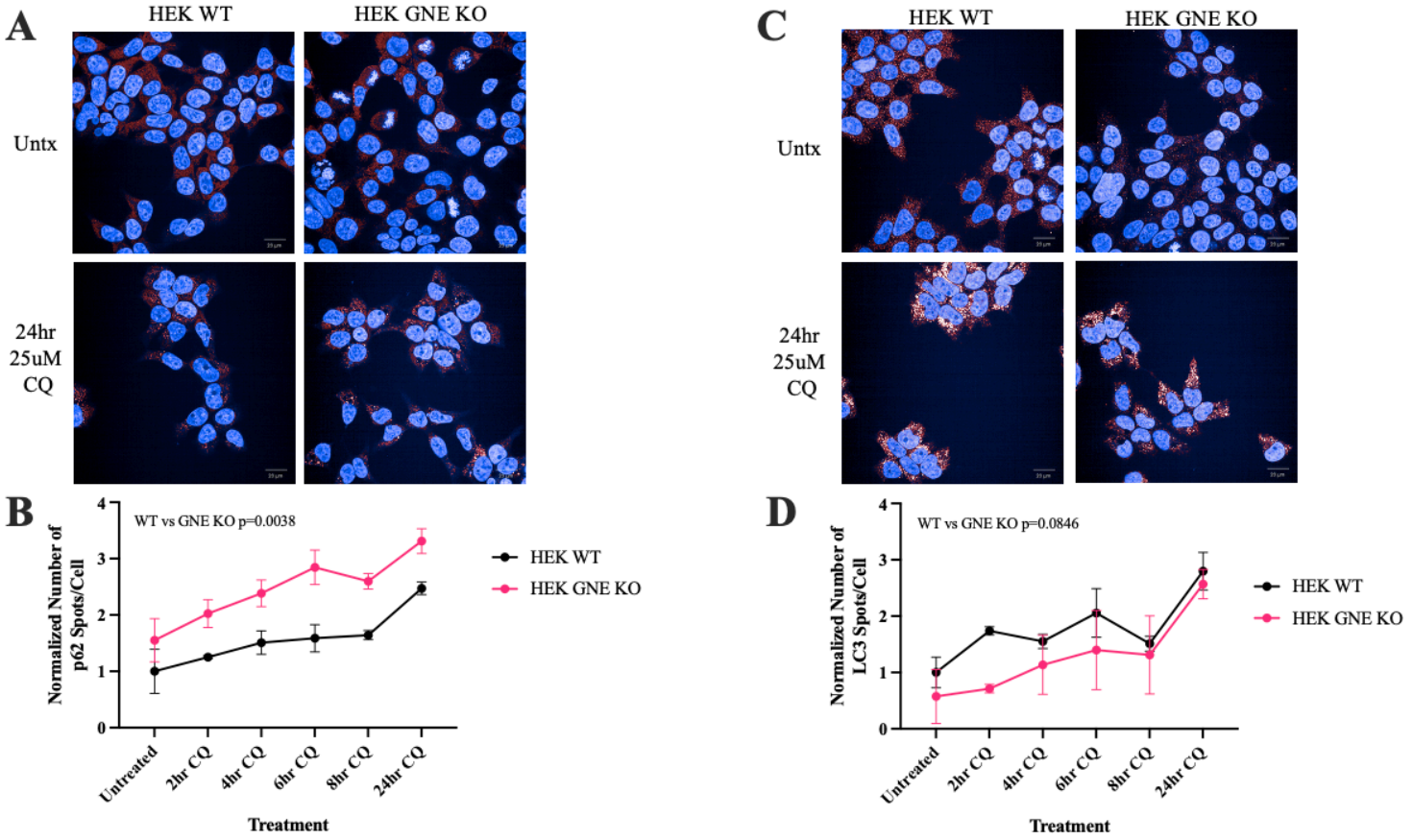


Figure 5

Time-course immunofluorescence analysis of autophagy markers p62 and LC3 in chloroquine-treated HEK cells.

A) p62 staining in HEK WT and *GNE*KO cells treated with 25uM of chloroquine over 24 hours (red = p62, blue = Hoechst).

B) Quantification of p62 staining in HEK WT and *GNE* KO cells (n=3 (approx. 750 cells/well), 3 wells from a single plate)

C) LC3 staining in HEK WT and *GNE*KO cells treated with 25uM of chloroquine for between 2 and 24 hours (red = LC3, blue = Hoechst).

D) Quantification of LC3 staining in HEK WT and *GNE* KO cells (n=3 (approx. 750 cells/well), 3 wells from a single plate)

WT = wildtype; KO = knockout; CQ = chloroquine, Untx = untreated. Scale Bar 20um.

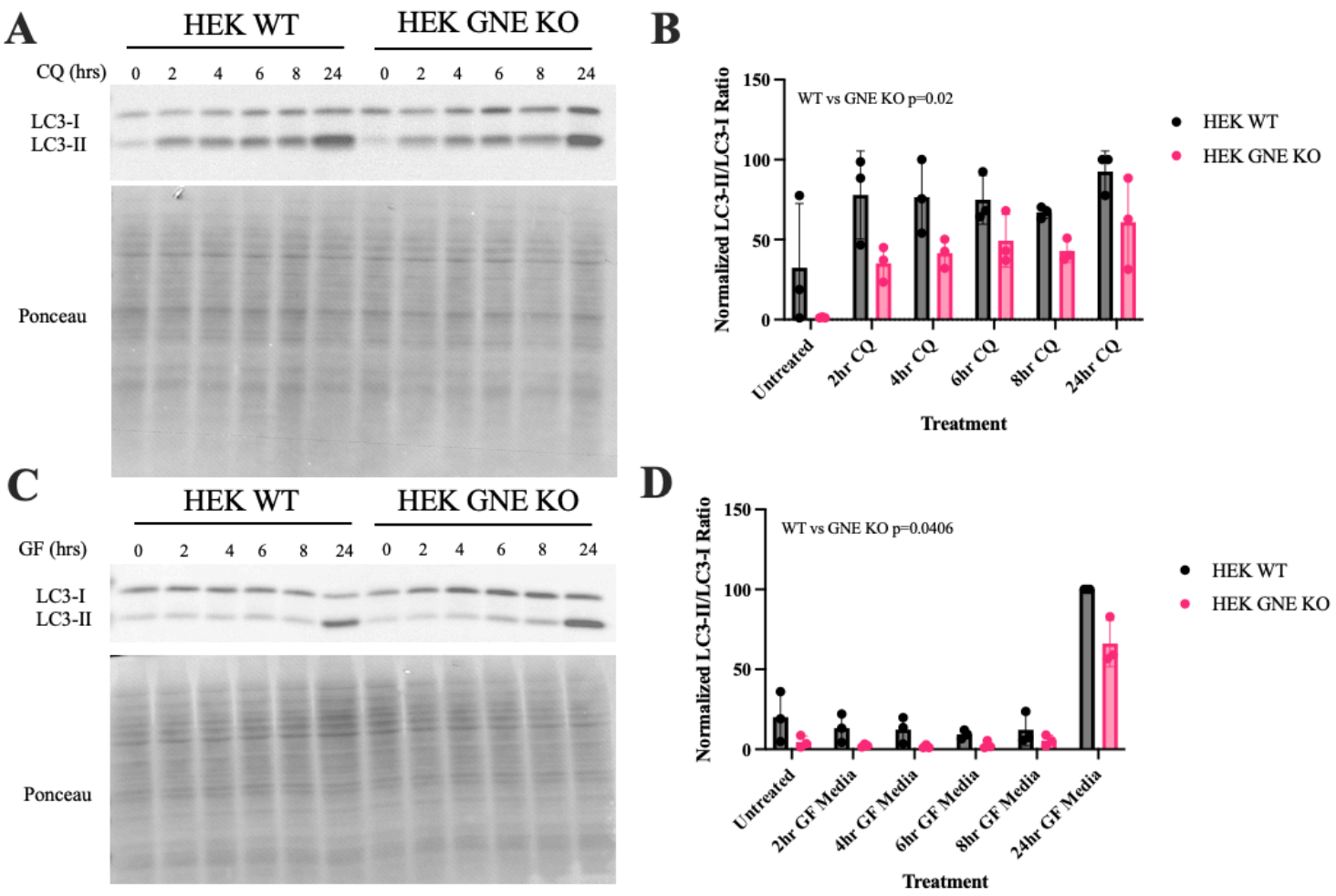


Figure 6

Time-course analysis of autophagy marker LC3 in chloroquine-treated and glucose-starved HEK cells.
A) Representative LC3 immunoblot in HEK WT and *GNE*KO cells treated with 25μM chloroquine over 24 hours.
B) Quantification of LC3-II/I ratio in chloroquine-treated HEK WT and *GNE*KO cells (n=3).
C) Representative LC3 immunoblot in HEK WT and *GNE* KO cells treated with 25μM chloroquine over 24 hours.
D) Quantification of LC3-II/I ratio in glucose-starved (GF) HEK WT and *GNE*KO cells (n=3).
WT = wildtype; CQ = chloroquine; GF = glucose-free

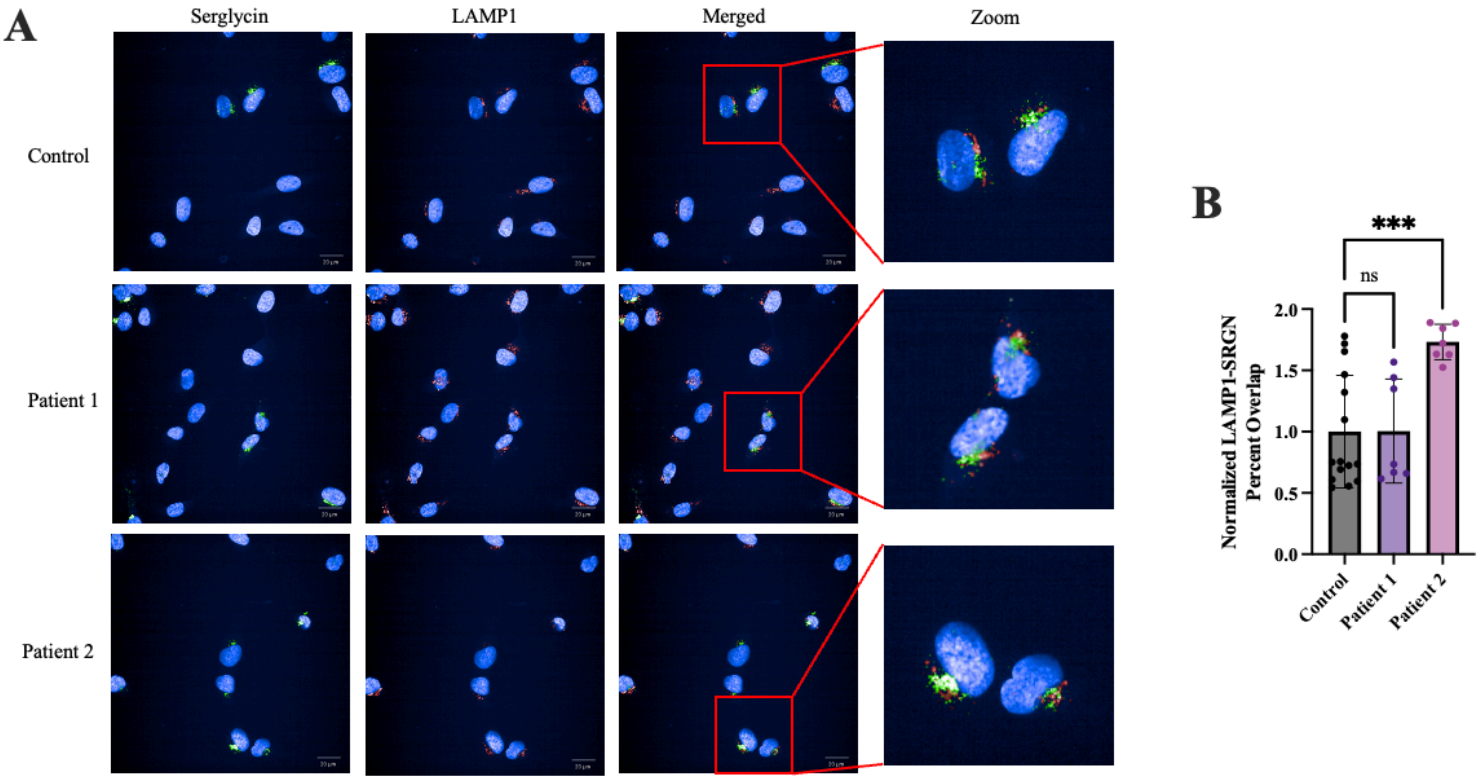


Figure 7

Overlap analysis of serglycin and LAMP1 in iPSC-derived myoblasts.
A) Representative immunofluorescence images of serglycin and LAMP1 staining in iPSC-derived myoblasts from control and two GNEM patients (green = serglycin, red = FAM134B, blue = Hoechst)
B) Quantification of serglycin-LAMP1 overlap (n=7-15 wells (approx. 700 cells/well); three control lines are combined into one control bar; replicates performed across 2 plates).

SRGN = serglycin. Scale Bar 20um.

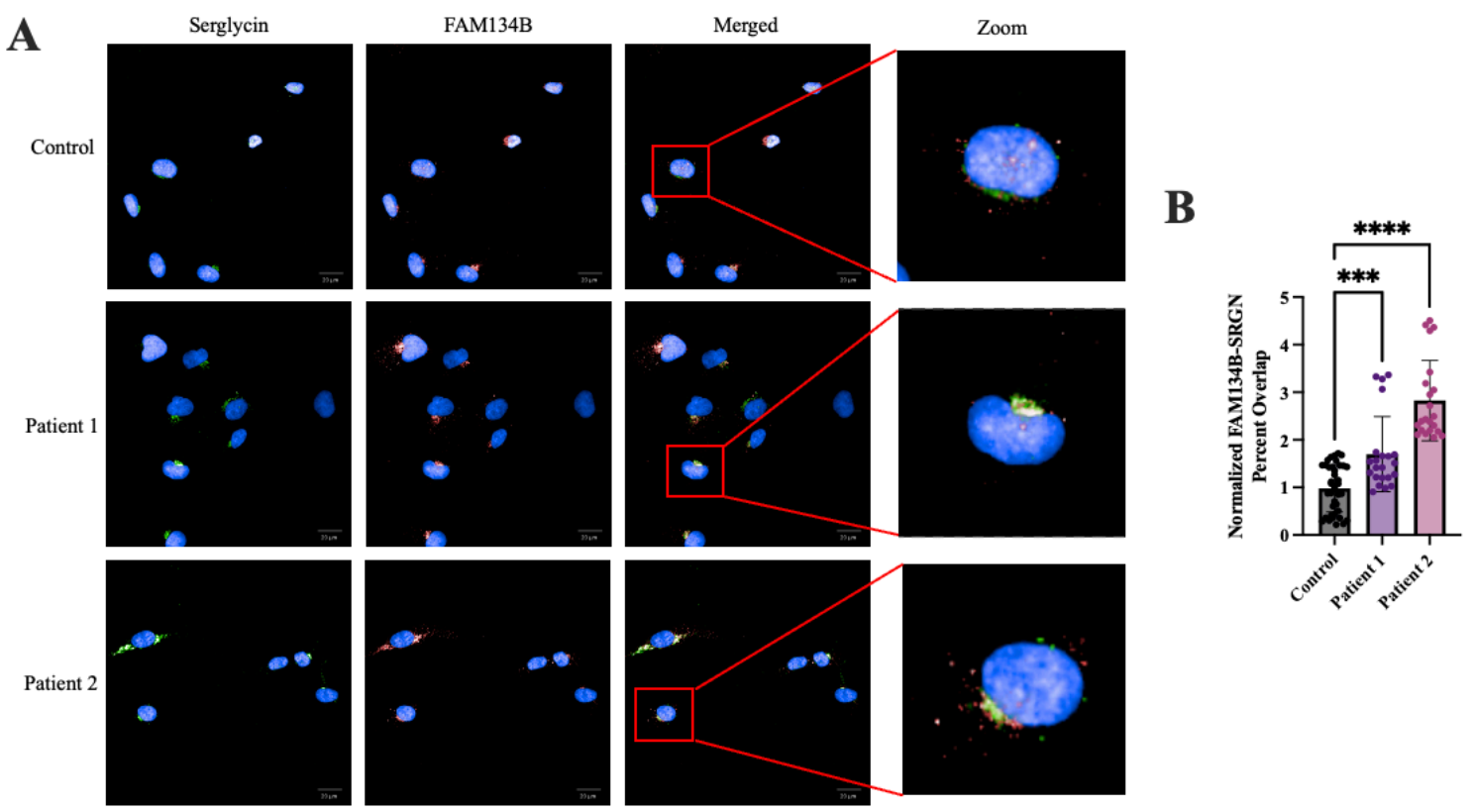


Figure 8

Overlap analysis of serglycin and FAM134B in iPSC-derived myoblasts.
A) Representative immunofluorescence images of serglycin and FAM134B staining in iPSC-derived myoblasts from control and two GNEM patients (green = serglycin, red = FAM134B, blue = Hoechst) B) Quantification of serglycin-FAM134B overlap (n=22-39 wells (approx. 750 cells/well); three control lines are combined into one control bar; replicates performed across 3 plates).

SRGN = serglycin. Scale Bar 20um.

Supplementary Files

This is a list of supplementary files associated with this preprint. Click to download.

- SupplementalDoc.docx